HHS Public Access

Author manuscript

Burns. Author manuscript; available in PMC 2018 September 16.

Published in final edited form as:

Burns. 2006 September ; 32(6): 755–764. doi:10.1016/j.burns.2006.01.011.

Tc-99m pyrophosphate imaging of poloxamer-treated electroporated skeletal muscle in an in vivo rat model★

Kenneth L. Matthews II[a,*], **John N. Aarsvold**[b,c], **Robert A. Mintzer**[c], **Chin-Tu Chen**[d], and **Raphael C. Lee**[e,1,**]

[a]Department of Physics and Astronomy, Louisiana State University, 202 Nicholson Hall, Baton Rouge, LA 70803, United States

[b]Nuclear Medicine Service, Atlanta Veterans Affairs Medical Center, United States

[c]Department of Radiology, Emory University, United States

[d]Department of Radiology, The University of Chicago, United States

[e]Department of Surgery, The University of Chicago, 5841 S. Maryland Avenue, MC 6035, Chicago, IL 60637, United States

Abstract

Objective—This study investigates whether ^{99m}Tc pyrophosphate (PYP) imaging provides a quantitative non-invasive assessment of the extent of electroporation injury, and of the effect of poloxamer in vivo on electroporated skeletal muscle.

Methods—High-voltage electrical shock was used to produce electroporation injury in an anesthetized rat's hind limb. In each experiment, the injured limb was treated intravenously by either poloxamer-188, dextran, or saline, and subsequently imaged with ^{99m}Tc PYP. The radiotracer's temporal behavior among the experimental groups was compared using curve fitting of time–activity curves from the dynamic image data.

Results—The washout kinetics of ^{99m}Tc PYP changed in proportion to the electric current magnitude that produced electroporation. Also, ^{99m}Tc PYP washout from electroporated muscle differed between poloxamer-188 treatment and saline treatment. Finally, 10-kDa dextran treatment of electroporated muscle altered ^{99m}Tc PYP washout less than poloxamer-188 treatment.

Conclusions—Behavior of ^{99m}Tc PYP in electroporated muscle appears to be an indicator of the amount of electroporation injury. Compared to saline, intravenous polaxamer-188 treatment reduced the amount of ^{99m}Tc PYP uptake. Coupled to results showing poloxamer-188 seals ruptured cellular membranes, lessens the extent of electroporation injury and improves cell viability, ^{99m}Tc PYP imaging appears to be a useful in vivo monitoring tool for the extent of electroporation injury.

★This work was conducted in accordance with institutional animal care and use policies and radiation protection practices.

*Corresponding author: Tel.: +1 225 578 2740; fax: +1 225 578 0824. **Corresponding author. Tel.: +1 773 702 6302; fax: +1 773 702 1634.

[1]The founder of Maroon Biotech; owned in part by The University of Chicago, Maroon Biotech is the licensee of patents derived from Dr. Lee's research on poloxamer applications to burn injury.

Keywords

Tc-99m pyrophosphate; Electrical injury; Electroporation; Poloxamer-188; Small animal imaging

1. Introduction

Since the development of electrical devices and electrical power distribution systems, electrical injury has been a serious problem [1]. Massive trauma can result from high-voltage shock by power–frequency electrical currents [2]. In biological tissues, the severity of response to electrical injury is related to the current involved. Responses range from muscle twitch and mild pain at small current to cardiac defibrillation at high currents [3]. Nerves and muscles are particularly susceptible to damage from electric shock, in part because of the extreme voltage gradients that can occur along these long cells. Burns and cellular disruption result directly from heat generated by an electric arc and the passage of electric current over and through the body, as well as from hot or burning debris [1]. Neuropsychological disorders can result both from physical trauma and emotional reaction to the injury [4,5]. A variety of approaches are used for the treatment of electrical injury, including fluid resuscitation, metabolic and respiratory support, surgical debridement, and skin grafting [6–8]. New therapeutic methods, such as immunologic therapy and artificial skin materials, may provide significant benefit. Basic research into the mechanisms of electrical injury is providing new insight into cellular-level approaches for limiting and repairing damage.

Historically, the damage from high-voltage injury was thought to be a direct result of heat production as current passes through tissue. Heating causes macromolecules to deform and become unable to perform their cellular functions; this can disrupt cellular metabolism and compromise structural integrity, resulting in cell death. Nerve cells typically have low resistivity, decreasing the likelihood of heating, but nerve cells are particularly susceptible to electrical injury. It is not uncommon for electrical shock victims to present with deep muscle and nerve damage, simultaneous with minimal signs of thermal injury at the site of contact [9,10]. This suggests the presence of damage mechanisms in addition to thermal damage [11].

Electroporation has been shown to be another cause of damage in high-voltage electrical injury [12,13]. One postulated mechanism is that field gradients during electric shock force polar water molecules into molecular-scale defects in the cellular membrane; the result is enlargement of the defects to form pores [14]. In electroporated tissues, cellular membranes are perforated, interfering with normal metabolic function. If the membrane damage can be patched, the cell may be able to resume functioning and survive the injury. Poloxamer, a type of surfactant, appears to form a suitable patch [15].

Poloxamers are non-toxic nonionic surface-active triblock copolymers [16]. Poloxamer’s structure, with a hydrophobic region bracketed by hydrophilic regions, has similarities to the phospholipid bilayer that comprises cellular membranes. Research indicates poloxamers associate themselves with a damaged membrane, coating exposed hydrophobic regions of the membrane and plugging water-enlarged pores [15,17]. Shielded from degradatory

influences, the cell would be provided the opportunity to recover, repair the membrane damage, and resume normal function.

The potential therapeutic effects of poloxamer-188 have been reported by a variety of researchers for a variety of types of tissue injury. Poloxamer-188 has been shown to limit the damage from electroporation to membranes [15,18] and to improve tissue viability [15,19]. Poloxamer-188 increases capillary circulation in several types of injuries [19,20]. Poloxamer-188 has also been reported to limit damage and improve recovery from mechanical, chemical, thermal, and radiation damage as well as ischemia-reperfusion injury in a variety of tissue types that include neurons, muscles, and heart [21–27]. The bulk of studies have investigated the effects of poloxamer-188 in vitro or in animal models. The literature includes some human case studies, as well as evident interest in using poloxamers in conjunction with electroporation as a tool for transmembrane drug delivery.

1.1. Radiotracer imaging of electrical injury

A number of trauma types can damage skeletal muscle and other soft tissues. Besides electrical injury, frostbite, ischemia and infections result in soft tissue injury. A variety of diagnostic methods are used commonly to evaluate soft tissue injury. These include visual assessment, histological and blood chemistry analysis, and radiological imaging.

Magnetic resonance imaging (MRI) is a valuable diagnostic tool because it provides exceptional delineation of soft tissues compared to other types of radiological imaging. The utility of MRI for electrical injury has been reported in several instances [28–32]. The detail visible from MRI can help to guide the surgeon in removal of tissue; MRI also visualizes the extent of deep tissue damage without the need for invasive exploration.

Functional imaging is also useful for assessing soft tissue injury. Compared to the anatomical visualization provided by MRI and CT scans, functional images show the physiological behavior of an organ system. With appropriate techniques, factors such as tissue perfusion, inflammation, metabolism and necrosis can be visualized. While techniques such as functional MRI have not yet been reported for assessing soft tissue damage, radiotracer imaging has been used extensively for assessment of soft tissue injury [33–36]. A number of tracers, particularly ^{99m}Tc-labeled phosphonates and ^{99m}Tc pyrophosphate (PYP), accumulate in damaged soft tissue [37–39]. The degree of tracer accumulation is often a good index of the extent of tissue damage [40–42].

Over the past two decades, radiotracer imaging has been used to assess the extent of damage in electrical injury victims [43–48]. Radiotracer imaging can delineate necrotic regions from viable tissue by visualizing the altered metabolism or function in these regions. In many cases, areas of abnormal tracer uptake may not appear visually necrotic until hours or days after the injury. The results of radiotracer imaging can assist in planning the surgical and therapeutic management of an injury [49]. A variety of radiopharmaceuticals are or could prove useful for clinical imaging of electrical injury of soft tissues, including ^{99m}Tc PYP, ^{99m}Tc hexakis-2-methoxyisobutylisonitrile (MIBI), ^{133}Xe, and ^{18}F-fluorodeoxyglucose (FDG).

Our study reports on ^{99m}Tc PYP imaging of electroporation injury in an in vivo rat model. Alterations in ^{99m}Tc PYP kinetics caused by differing amounts of electroporation injury and different therapeutic agents were assessed by region of interest (ROI) analysis of dynamic radiotracer images and curve fitting. The purpose of our study was to determine if ^{99m}Tc PYP imaging provides a quantitative non-invasive assessment of the extent of electroporation injury and of the effect of poloxamer treatment on electroporated skeletal muscle.

2. Materials and methods

Fig. 1 shows the experimental equipment used in this work. The components are described in the following sections.

2.1. In vivo model of electroporation

This research utilized the in vivo model of electroporation developed by Block et al. [50]. This model provides a means to study electroporation in the absence of thermal damage, in the skeletal muscle of the hind limb of an anesthetized rat; our study focuses on visualizing damage to the *biceps femoris* muscle. Briefly, the centerpiece of the model is a female Sprague–Dawley rat kept fully anesthetized by continuous intraperitoneal infusion of a mixture of ketamine and xylazine. The animals used in this work weighed 280–350 g and all were non-pregnant and free of disease. A jugular cannula introduced radiotracer, saline, and therapeutic agents directly into the bloodstream of the animal. All experiments were not survived; euthanasia at the end of the experiment was accomplished with an overdose of xylazine administered either through the jugular cannula or directly into the heart.

As in Block's model, electroporation damage was produced throughout the muscle of one hind limb by applying a sequence of high-voltage current-regulated dc electrical pulses from the ankle to the base of the tail [50]. Electric field strength of approximately 150 V/cm was delivered at a constant current between the ankle and base of the tail. The maximum available current was 1.85 A. The pulse duration was 4 ms, equivalent to the length of time that a 60 Hz sine wave exceeds its root-mean-square (rms) amplitude in each half-cycle. Twelve pulses were applied from the base of the tail to the ankle over a 2-min span; the 10-s interval between pulses minimizes heat accumulation in the limb.

2.2. High-resolution small-field-of-view gamma camera

The imaging system used in this work was a high-resolution small-field-of-view gamma camera [51]. The camera provides a 64 × 64 pixel, 4.8 cm × 4.8 cm field of view, sufficient to image one hind limb of the rats used in this study; a second camera was used to image the contralateral (unshocked) limb in some experiments. With its high-resolution collimator, the imaging resolution is 5.4 mm full-width-at-half-maximum at a 5 cm depth.

The camera software provides automated acquisition of dynamic image data; each image is 2 min in duration, with a 2.4 min interval between the start of successive images. (The 0.4-min lag was the length of time required by the operator to manually save each image to disk in a pre-automated version of the software; the lag was maintained to facilitate comparison with earlier imaging studies.) Region of interest (ROI) analysis and curve-fitting of the

dynamic image data was performed off-line using analysis programs written in the Interactive Data Language (IDL) software (Research Systems, Boulder, CO).

2.3. Selection of radiotracer

Four radiotracers were considered for use in this research. These were ^{99m}Tc PYP, ^{99m}Tc diethylenetriaminepentaacetate (DTPA), ^{99m}Tc hexakis-2-methoxyisobutylisonitrile (MIBI), and ^{201}Tl thallous chloride. Each tracer has biological characteristics that make it potentially useful for imaging electroporation injury [52]. Technetium-99m PYP was selected as the best candidate radiotracer for imaging electroporation in the in vivo rat model.

Technetium-99m PYP is well known as a tracer for soft tissue injury [37–40]. It accumulates in damaged soft tissue, clears moderately quickly from undamaged soft tissue, and accumulates over time in bone. The biggest drawback to using ^{99m}Tc PYP is that the mechanism of its accumulation in damaged tissue is not well understood; it is believed to follow calcium in cellular function [53–55]. The exact structure of ^{99m}Tc PYP is not known; PYP forms a complex with technetium in the presence of a tin catalyst, but the number of PYP molecules per technetium atom has never been determined conclusively. Estimates range from one to five PYP molecules per technetium atom; it appears possible that the number is variable.

2.4. Therapeutic agents

The two therapeutic agents investigated in this work were poloxamer and dextran; saline was used as a control. Poloxamer-188 (Pluronic F68, BASF Corp., Florham Park, NJ) was examined at 17 and 68 mg dosages. The dextran experiments used 10 or 40 kDa neutral dextran (Sigma Chemicals, St. Louis, MO) at a 17 mg dosage. Ten kilodaltons dextran is similar in molecular weight to poloxamer-188; 40 kDa dextran is used clinically as a plasma expander in electrical injury victims. Saline was used in control experiments. Saline-treated unshocked muscle provided a normal baseline for comparison. In all cases, a solution volume of 0.4 ml (e.g., 68 mg of poloxamer-188 was dissolved in saline to produce a volume of 0.4 ml) was injected through the jugular cannula. Table 1 summarizes the parameters of the experimental protocol, including the numbers of animals in each experimental group.

The blood volume of a 300 g rat is approximately 17 ml. Thus, the approximate effective blood concentrations in the groups of experimental animals treated with 17 and 68 mg of poloxamer-188 are 1 and 4 mg/ml, respectively. A blood concentration of 1 mg/ml approximates the dosage that might be administered to patients in clinical trials of poloxamer therapy for electroporation. A 4 mg/ml concentration is close to critical micelle concentration for poloxamer-188; above this concentration, poloxamer is expected to form micelles, thereby potentially limiting interactions with ruptured cell membranes.

2.5. Imaging protocol

The experimental protocol for investigating poloxamer calls for the investigative agent to be injected through the jugular cannula at ten minutes after shock. In control experiments, saline was injected at this time. Technetium-99m PYP was injected through the cannula at 30 min post-shock. An activity of 37 × 7.4 MBq (1.0 × 0.2 mCi) in 0.4 ml saline was

injected. The small gamma camera acquired serial, posterior view images of the shocked hind limb. Each image was 2 min in duration with a new image starting every 2.4 min. The imaging phase of each experiment extended for 3.5 h post-shock; 88–90 images were usually obtained. During data analysis, the dynamic image data were reviewed. If a cine image loop showed that the limb moved or that radioactive urine leaked into the field of view, the data for that experiment were rejected from further analysis.

Experiments that had excessive vascular damage in the hind limb were excluded also. While the focus of this research is electroporation of skeletal muscle, the electroporation protocol cannot avoid doing some damage to the vasculature of the shocked limb. In some experiments, the amount of tracer uptake in a shocked limb would never rise above the level seen in unshocked limbs. This lack of tracer delivery was due most likely to compromised vasculature. To assess the extent of vascular damage in each experiment, lissamine green was injected through the jugular catheter 10 min before euthanasia. Lissamine green is a dye whose distribution depends on tissue perfusion; poor staining of the muscle indicates compromised vasculature. After euthanasia, the *biceps femoralis* muscle of the shocked and contralateral limbs would be exposed and visually inspected. If the shocked muscle showed little staining compared to the unshocked limb, the vasculature was deemed compromised and the data rejected. We noted the correlation that experiments where the muscle of the shocked limb showed little staining with lissamine green, the tracer uptake consistently was below unshocked saline-treated levels at all times. Note that the lissamine green observation was always recorded before any image data analysis; rejection of a data set was based on the lissamine green staining, not on the radiotracer image data.

The research plan was to acquire ten experiments at 1.85 A of applied current for each type and concentration of therapeutic agent and five experiments each for the unshocked data sets and the data sets that compared the other levels of applied current. Experiments where compromised vasculature was noted via lissamine green staining, were not counted towards each category's total and an additional experiment was done in these cases. Instances of limb movement or radioactive urine in the field of view were identified later during the data analysis, and additional experiments were not done to replace these. The final numbers of experiments in each data set are noted in the legends of the figures and in Table 1. Four additional experiments were collected for the 17 mg 40 kDa dextran data set while training a new lab employee; these experiments were included in the analysis because there were no specific procedural issues to justify excluding them from the analysis. Approximately 80 experiments in total were performed to obtain the data reported here.

2.6. ROI analysis

ROI analysis was used to extract time–activity curves (TACs) from the dynamic image data. Using display and analysis code written in IDL, an 8 × 7-pixel (6 mm × 5.25 mm) ROI positioned over the *biceps femoralis* muscle was used to compute a TAC for each experiment. The TACs were positioned using a composite image produced by summing all images from the dynamic data set. The location of the knee and the outline of soft tissue of the hind limb were clearly visible in the composite image; the ROI was placed visually over the soft tissue below the bones of the lower limb, as shown in Fig. 2. The TACs from

individual experiments were averaged to yield a mean curve for each data set. To provide a quantitative characterization of the ROI data for ^{99m}Tc PYP, the average TACs were fit by a least-squares algorithm to a simple mathematical model. The fitting function uses an exponential decay on a constant background level, with the form:

$$f(t) = A \exp(-Bt) + C \quad (1)$$

to describe the washout of tracer. Tracer uptake was not modeled; uptake occurs rapidly during the first two minutes after radiotracer injection and was not recorded by our imaging protocol.

The fitted parameters for the curves were compared statistically to determine the level of significance of differences in the fitted parameters. Student's *t*-value was computed for pairs of corresponding average fitted parameters between the different data sets. A level of $p < 0.01$ was chosen to indicate the level of significance. This relatively stringent level was chosen because multiple comparisons between data sets are made. Each data set is compared to six other data sets; consequently, the selected *p*-value corresponds to significance approximately at a 95% confidence level.

3. Results

Technetium-99m PYP is known to accumulate in damaged soft tissue, and the experimental validation of the in vivo electroporation model [50] confirmed that ^{99m}Tc PYP accumulates in electroporated tissue. Fig. 3 shows that the TAC magnitudes for ^{99m}Tc PYP are proportional to the current magnitude used to produce electroporation and, thus, indicative of the amount of electroporation injury. This result indicates that ^{99m}Tc PYP can serve as an index to the extent of electroporation injury. Higher uptake means more damage and lower uptake means less damage. This provides a means for in vivo assessment of the effect of poloxamer-188 on electroporated muscle. If membrane damage is being reduced by poloxamer, the uptake of PYP should be less than in muscle to which poloxamer was not administered.

To rule out the possibility that any observed change in ^{99m}Tc PYP kinetics in poloxamer-treated muscle is caused by direct molecular interaction of poloxamer with PYP, independent of the presence of tissue damage, a set of poloxamer-treated unshocked experiments were conducted. Fig. 4 shows the average TAC for unshocked muscle treated with 17 mg poloxamer-188. The TAC magnitude is marginally higher at all times than that for unshocked muscle treated with saline. This slight increase most likely results from poloxamer-188 acting as a plasma expander [56]. Therefore, any perceived change in tracer behavior includes a small fractional increase due to this effect. In addition, this effect is opposite in magnitude to the observed changes in PYP uptake in poloxamer-treated shocked muscle (see below), giving confidence that the observed decreases in the poloxamer-treated shocked experiments are due primarily to the effects of poloxamer on the damaged tissue, rather than from direct interaction between the ^{99m}Tc PYP and the poloxamer. One could remove the effect of this plasma-expansion increase from the other data sets by subtracting

away the average unshocked-poloxamer-treated TAC. However, the increase in TAC magnitude is small (relative to the large increase seen in shocked muscle) so we chose not to implement a correction to the other image data for this effect.

Shown in Fig. 5 are average TACs for ^{99m}Tc PYP in unshocked saline-treated, shocked saline-treated and shocked poloxamer-treated muscle. It is immediately apparent that the magnitude of PYP uptake in electroporated muscle is substantially higher than in normal muscle. Additionally, while the temporal behavior is similar for saline-treated electroporated and saline-treated normal muscle, the behavior appears different for electroporated muscle that has been treated with 17 mg of poloxamer-188. The relatively constant value of the TAC for poloxamer treatment contrasts sharply with the exponential shape of the saline-treated curves. One also sees that treatment with 68 mg of poloxamer-188 results in a TAC that is similar to that for saline-treated muscle. A pertinent question here is what causes this different behavior of PYP in 17 mg poloxamer-188 treated muscle. Ideally, the altered kinetics are due to sealing of ruptured membranes by poloxamer-188, leading to improved long-term cell viability.

Fig. 6 illustrates the results of treating electroporated muscle with 17 mg of 10 or 40 kDa neutral dextran. Forty kilodaltons dextran causes an initial marginal decrease in tracer uptake compared to saline, but little difference is apparent at 4 h post-shock. A larger initial decrease is seen with 10 kDa dextran but the difference is negligible 4 h post-shock. Compared to shocked saline-treated muscle, tracer washout appears slightly faster for 40 kDa dextran and substantially faster for 10 kDa dextran. Fig. 7 shows that treatment with 17 mg of 10 kDa dextran does not alter the kinetics of ^{99m}Tc PYP as much as treatment with 17 mg of poloxamer-188 does.

Table 2 lists the fitted values from the average curves; significance levels for pairs of average parameters from individual fitted curves are given in Table 3. Entries with $p < 0.01$ (corresponding approximately to a 95% confidence level for multiple comparisons between the different experimental groups) are presented in bold typeface. One of the most notable results is that the 17 mg poloxamer-treated data do not show any particular difference in its *B*-parameter from the other data sets; this indicates that the washout rate is unchanged, so the altered appearance of the curve is due to a change in initial magnitude (*A*-parameter). Another observation is that the unshocked saline-treated data are not significantly different in any of the fitting parameters from the unshocked poloxamer-treated data. Finally, one notes that the 1.85 A shocked saline-treated and 1.85 A shocked poloxamer-treated data are marginally different at best in the *C*, or baseline, parameter.

4. Discussion

Our study demonstrates that the in vivo electroporation model is a useful tool for the study of the basic pathophysiologic process of electroporation. Radiotracer imaging of the in vivo model provides a means for quantifying the extent of electroporation injury and the effects of poloxamer-188 and other potential therapeutic agents on electroporated muscle.

Because of its history as a tracer for soft-tissue injury, ^{99m}Tc PYP was expected to be a good choice for use in the electroporation research. The curves in Fig. 5 show that the PYP TAC is substantially different in electroporated muscle treated with 17 mg poloxamer-188 than in saline-treated electroporated muscle. In particular, PYP reaches a steady-state level for the poloxamer case that is noticeably less than the plateau level for saline treatment. However, one notes that at the ~95% confidence level chosen for comparison, the A and C parameters for these data sets are not significantly different. Based on the apparent substantial difference in the TACs, one expects that with the addition of more experiments to these data sets, the errors bars will decrease in magnitude and the level of statistical significance will improve.

In unshocked muscle, PYP kinetics are not significantly different if the muscle is treated with 17 mg poloxamer-188 than if it is treated with saline. The baseline parameters for the unshocked data sets are significantly different from all the shocked data sets, as one expects visually from the TACs in Figs. 4–7.

For all data sets, the rate parameters for the TACs are not significantly different between any of the data sets. For the exponential-plus-constant-background fitting function, the B-parameter of the fitted TACs is not significantly different between either unshocked saline-treated and shocked saline-treated experiments or shocked saline-treated and shocked poloxamer-treated experiments. This indicates that the washout mechanism of PYP is unaltered by shocking or by treatment with poloxamer-188, while the mechanisms driving uptake and the equilibrium distribution are affected.

4.1. Radiotracers for future investigation

Technetium-99m PYP was chosen for this work primarily because of its extensive history as a tracer for soft tissue injury. However, ^{99m}Tc PYP was not the only possible choice. In addition to other tracers discussed in Ref. [52], ^{133}Xe and ^{18}F-FDG could be useful for clinical and research imaging of electroporation, but these were not considered practical for the current research. FDG has been reported for clinically assessing skeletal muscle viability [57]. Although, the shielding and collimation of the small gamma camera used in this study were not designed for 511 keV imaging, FDG imaging of the in vivo model of electroporation seems an interesting prospect, given the current availability of small animal PET scanners (e.g., microPET, CTI Molecular Imaging, Knoxville, TN). Xenon-133 was rejected as impractical for this investigation because of its long half-life and difficulties in achieving a specific activity of aqueous ^{133}Xe that was high enough to calibrate the small gamma camera system.

Technetium-99m-labeled dextran and ^{99m}Tc-labeled poloxamer potentially would be ideal tracers for research and clinical investigations. Technetium-99m poloxamer would be especially attractive for investigating the interaction of poloxamer with electroporated membranes. While dextran has been successfully radiolabeled with ^{99m}Tc [58], the feasibility of developing ^{99m}Tc-labeled poloxamer for in vivo imaging is an open question; ^{18}F-labeled poloxamer for PET imaging may be more reasonable.

5. Conclusion

In summary, the in vivo electroporation model [50] showed that electroporation without significant Joule heating can occur during high-voltage electrical shock. The model is clinically realistic and provides a means for studying the basic pathophysiology of electroporation injury. Our study used the in vivo model to study the effect of poloxamer on electroporated muscle. Intravenous injection of poloxamer-188 significantly lessens the amount of ^{99m}Tc PYP retained by electroporated skeletal muscle. Taken in conjunction with in vitro research reported in the literature [17,18,59], as well as in vivo studies that indicated poloxamer-188 minimizes damage and improves viability [15,19,23,25], the results from our work indicate that poloxamer may have a beneficial therapeutic effect on electroporated cells. Radiotracer imaging of electroporated skeletal muscle appears to be a viable non-invasive method for judging the extent of injury and tissue viability. Further work on modeling the kinetics of ^{99m}Tc PYP in poloxamer-treated electroporated tissues may provide the ability to quantify extent of injury from dynamic image data.

Acknowledgments

Support for this work was provided by the Department of Energy through grant no. DE-FG02-86ER60418 and by the Electrical Power Research Institute. Jeffrey Yap, PhD, provided advice on performing the statistical analysis on the image data. Grigory Abramov assisted with animal preparation for some of the experiments; the nuclear medicine technologists in the Department of Radiology prepared all the radiopharmaceuticals used in this work. Finally, the authors thank Thomas Block for his efforts in developing the in vivo model of electroporation. This work is dedicated to the memory of Malcolm Cooper, MD, our teacher, colleague and friend.

References

1. Bernstein T. Electrical injury: Electrical engineer’s perspective and an historical review. In: Lee RC, Capelli-Schellpfeffer M, Kelly KM, editorsAnn NY Acad Sci. Vol. 720. 1994. 1–10. Electrical injury: a multidisciplinary approach to therapy, prevention, and rehabilitation
2. Lee RC, Cravalho EG, Burke JF. Electrical trauma: the pathophysiology, manifestations, and clinical management. Cambridge: Cambridge University Press; 1992.
3. Reilly JP. Scales of reaction to electric shock. In: Lee RC, Capelli-Schellpfeffer M, Kelly KM, editorsAnn NY Acad Sci. Vol. 720. 1994. 21–37. Electrical injury: a multidisciplinary approach to therapy, prevention, and rehabilitation
4. Kelley KM, Pliskin N, Meyer G, Lee RC. Neuropsychiatric aspects of electrical injury: The nature of psychiatric disturbance. In: Lee RC, Capelli-Schellpfeffer M, Kelly KM, editorsAnn NY Acad Sci. Vol. 720. 1994. 213–8. Electrical injury: a multi-disciplinary approach to therapy, prevention, and rehabilitation
5. Duff K, McCaffrey RJ. Electrical injury and lightning injury: a review of their mechanisms and neuropsychological, psychiatric, and neurological sequalae. Neuropsychol Rev. 2001; 11:101–16. [PubMed: 11572471]
6. Waymack JP, Rutan RL. Recent advances in burn care. In: Lee RC, Capelli-Schellpfeffer M, Kelly KM, editorsAnn NY Acad Sci. Vol. 720. 1994. 230–8. Electrical injury: a multi-disciplinary approach to therapy, prevention, and rehabilitation
7. Hammond JS, Ward CG. High-voltage electrical injuries: management and outcome of 60 cases. South Med J. 1988; 81:1351–2. [PubMed: 2847326]
8. Lee RC, Dougherty W. Electrical injury: mechanisms, manifestations, and therapy. IEEE Trans Dielectr Electr Insul. 2003; 10:810–9.
9. Lee RC, Kolodney MS. Electrical injury mechanisms: dynamics of the thermal response. Plast Reconstr Surg. 1987; 80:663–71. [PubMed: 3671557]

10. Smith MA, Muehlberger T, Dellon AL. Peripheral nerve compression associated with low-voltage electrical injury without associated significant cutaneous burn. Plastic Reconstruct Surg. 2002; 109:137–44.
11. Lee RC, Gaylor DC, Bhatt D, Israel DA. Role of cell membrane rupture in the pathogenesis of electrical trauma. J Surg Res. 1988; 44:709–19. [PubMed: 3379948]
12. Bhatt DL, Gaylor DC, Lee RC. Rhabdomyolysis due to pulsed electric fields. Plastics Reconstruct Surg. 1990; 86:24–34.
13. Lee RC, Kolodney MS. Electrical injury mechanisms: electrical breakdown of cell membranes. Plastics Reconstruct Surg. 1987; 80:672–9.
14. Abidor IG, Arakelyan VB, Chernomordik LV, Chizmadzhev YA, Pastushenko VF, Tarasevick MR. Electric breakdown of bilayer lipid membranes. I. The main experimental facts and their qualitative discussion. Bioelectrochem Bioenerget. 1979; 6:37–52.
15. Lee RC, River P, Pan F-S, Ji L, Wollmann RL. Surfactant-induced sealing of electropermeabilized skeletal muscle membranes in vivo. Proc Natl Acad Sci USA. 1992; 89:4524–8. [PubMed: 1584787]
16. Schmolka IR. Artificial skin. I. Preparation and properties of pluronic F-127 gels for treatment of burns. J Biomed Mater Res. 1972; 6:571–82. [PubMed: 4642986]
17. Maskarinec SA, Hannig J, Lee RC, Lee KYC. Direct observation of poloxamer 188 insertion into lipid monolayers. Biophys J. 2002; 82:1453–9. [PubMed: 11867460]
18. Sharma V, Stebe K, Murphy JC, Tung L. Poloxamer 188 decreases susceptibility of artificial lipid membranes to electroporation. Biophys J. 1996; 71:3229–41. [PubMed: 8968593]
19. Basakaran H, Toner M, Yarmush ML, Berthiaume F. Poloxamer-188 improves capillary blood flow and tissue viability in a cutaneous burn wound. J Surg Res. 2001; 101:56–61. [PubMed: 11676555]
20. Hsu LL, Liu XW, Pierangeli S, et al. Microcirculatory effects of poloxamer 188 in transgenic sickle cell mice. Blood. 2002; 100:664A.
21. Mezrow CK, Mazzoni M, Wolfe D, Shiang HH, Litwak RS, Griepp RB. Poloxamer-188 improves neurologic outcome after hypothermic circulatory arrest. J Thoracic Cardiovasc Surg. 1992; 103:1143–6.
22. Merchant FA, Holmes WH, Capelli-Schellpfeffer M, Lee RC, Toner M. Poloxamer 188 enhances functional recovery of lethally heat-shocked fibroblasts. J Surg Res. 1998; 74:131–40. [PubMed: 9587351]
23. Kelly RF, Hursey TL, Patel RB, Parrillo JE, Schaer GL. Effect of poloxamer 188 on collateral blood flow, myocardial infarct size, and left ventricular function in a canine model of prolonged (3-h) coronary occlusion and reperfusion. J Thrombosis Thrombolysis. 1998; 5:239–47.
24. Watanabe M, Okada T. Lysophosphatidylcholine-induced myocardial damage is inhibited by pretreatment with poloxamer 188 in isolated rat heart. Mol Cell Biochem. 2003; 248:209–15. [PubMed: 12870676]
25. Curry DJ, Wright DA, Lee RC, Kang UJ, Frim DM. Surfactant poloxamer 188-related decreases in inflammation and tissue damage after experimental brain injury in rats. J Neurosurg. 2004; 101:91–6. [PubMed: 16206978]
26. Greenebaum B, Blossfield K, Hannig J, et al. Poloxamer 188 prevents acute necrosis of adult skeletal muscle cells following high-dose irradiation. Burns. 2004; 30:539–47. [PubMed: 15302418]
27. Serbest G, Horwitz J, Barbee K. The effect of poloxamer-188 on neuronal cell recovery from mechanical injury. J Neurotrauma. 2005; 22:119–32. [PubMed: 15665607]
28. Ohashi M, Koizumi J, Hosoda Y, Fujishiro Y, Tuyuki A, Kikuchi K. Correlation between magnetic resonance imaging and histopathology of an amputated forearm after electrical injury. Burns. 1988; 24:362–8.
29. Weissenburger J, Clement PF. MRI correlates of electrical injury. Arch Clin Neuropsychol. 1998; 13:134.
30. Kalita J, Jose M, Misra UK. Myelopathy and amnesia following accidental electrical injury. Spinal Cord. 2002; 40:253–5. [PubMed: 11987009]

31. Sahiner T, Kurt T, Bir LS, et al. Reversible hyperintense T2 MRI lesions of basal ganglia after an electrical injury. Burns. 2002; 28:607–8. [PubMed: 12220922]
32. Freeman CB, Goyal M, Bourque PR. MR imaging findings in delayed reversible myelopathy from lightning strike. Emerg Med J. 2004; 21:750–1. [PubMed: 15496717]
33. Brill DR. Radionuclide imaging of non-neoplastic soft tissue disorders. Semin Nucl Med. 1981; 11:277–88. [PubMed: 6272422]
34. Malki AA, El-Gazzar A, Ashqar T, Owunwanne A, Abdel-Dayem H. New technique for assessing muscle damage after trauma. J R Coll Surg Edinburgh. 1992; 37:131–3.
35. Mehta RC, Wilson MA. Frostbite injury: prediction of tissue viability with triple-phase bone scanning. Radiology. 1989; 170:511–4. [PubMed: 2911677]
36. Labbe R, Lindsay T, Gatley R, et al. Quantitation of postischemic skeletal muscle necrosis: histochemical and radioisotope techniques. J Surg Res. 1988; 44:45–53. [PubMed: 2447386]
37. Haseman MK, Kriss JP. Selective, symmetric, skeletal muscle uptake of Tc-99m pyrophosphate in rhabdomyolysis. Clin Nucl Med. 1985; 10:180–3. [PubMed: 2985322]
38. Delpassand ES, Dhekne RD, Barron BJ, Moore WH. Evaluation of soft tissue injury by Tc-99m bone agent scintigraphy. Clin Nucl Med. 1991; 16:309–14. [PubMed: 1647284]
39. Owunwanne A, Malki A, Sadek S, El-Gazzar A, Yacoub T, Abdel-Dayem HM. Investigative study of radiopharmaceuticals useful for imaging skeletal muscle injury in experimental animals. Am J Physiol Imag. 1989; 4:62–5.
40. Siegel BA, Engel WK, Derrer EC. ^{99m}Tc-diphosphonate uptake in skeletal muscle: a quantitative index of acute damage. Neurology. 1975; 25:1055–8. [PubMed: 1237823]
41. Timmons JH, Hartshorne MF, Peters VJ, Cawthon MA, Bauman JM. Muscle necrosis in the extremities: evaluation with Tc-99m pyrophosphate scanning—a retrospective review. Radiology. 1988; 167:173–8. [PubMed: 2831562]
42. Affleck DG, Edelman L, Morris SE, Saffle JR. Assessment of tissue viability in complex extremity injuries: utility of the pyrophosphate nuclear scan. J Trauma Injury Infect Crit Care. 2001; 50:263–9.
43. Chang LY, Yang JY. The role of bone scans in electric burns. Burns. 1991; 17:250–3. [PubMed: 1892562]
44. Lewis SE, Hunt JL, Baxter C, Hickey DC, Parkey RW. Identification of muscle damage in acute electrical burns with technetium-99m pyrophosphate (Tc-99m-PYP) scintigraphy. J Nucl Med. 1979; 20:646–7.
45. Sayman HB, Urgancioglu I, Uslu I, Kapicioglu T. Prediction of muscle viability after electrical burn necrosis. Clin Nucl Med. 1992; 17:395–6. [PubMed: 1587046]
46. Spencer RR, Williams AG Jr, Mettler FA Jr, Christie JH, Rosenberg RD, Weaver WD. Tc-99m PYP scanning following low voltage electrical injury. Clin Nucl Med. 1983; 8:591–3. [PubMed: 6317262]
47. Hunt JL, Lewis S, Parkey R, Baxter C. The use of technetium-99m stannous pyrophosphate scintigraphy to identify muscle damage in acute electric burns. J Trauma. 1979; 19:409–13. [PubMed: 448780]
48. Ino H, Chikamori T, Hatano T, et al. High-tension electrical injury to the heart as assessed by radionuclide imaging. Ann Nucl Med. 2002; 16:557–761. [PubMed: 12593421]
49. Hunt JL, Sato RM, Baxter C. Acute electric burns: current diagnostic and therapeutic approaches to management. Arch Surg. 1980; 115:434–8. [PubMed: 6987974]
50. Block TA, Aarsvold JN, Matthews KL, et al. The 1995 Lindberg award: Non-thermally mediated muscle injury and necrosis in electrical trauma. J Burn Care Rehab. 1995; 16:581–8.
51. Aarsvold JN, Mintzer RA, Yasillo NJ. , et al. A miniature gamma camera. In: Lee RC, Capelli-Schellpfeffer M, Kelly KM, editorsAnn NY Acad Sci. Vol. 720. 1994. 192–205. Electrical injury: a multidisciplinary approach to therapy, prevention, and rehabilitation
52. Matthews KL, , IIAarsvold JN, Mintzer RA. , et al. Radiotracers for imaging electroporation. In: Chen C-T, Lee RC, Shih J-X, Zhong M-H, editorsAnn NY Acad Sci. Vol. 888. 1999. 285–99. Occupational electrical injury: an international symposium

53. Shen AC, Jennings RB. Kinetics of calcium accumulation in acute myocardial ischemic injury. Am J Pathol. 1972; 67:441–52. [PubMed: 5033258]

54. Jung A, Bisaz S, Fleisch H. The binding of pyrophosphate and two diphosphonates by hydroxyapatite crystals. Calcif Tissue Res. 1973; 11:269–80. [PubMed: 4350498]

55. Lessem J, Polimeni PI, Page E, Resnekov L, Harper PV, Stark V. Accumulation of technetium-99m pyrophosphate in experimental infarctions in the rat. Cardiovasc Res. 1980; 14:352–9. [PubMed: 6253070]

56. Hymes AC, Safavian MH, Arbulu A, Baute P. A comparison of Pluronic F-68, low molecular weight dextran, mannitol, and saline as priming agents in the heart-lung apparatus. I. Pluronic F-68: first use as a plasma substitute. J Thorac Cardiovasc Surg. 1968; 56:16–22. [PubMed: 5663128]

57. Smith GT, Wilson TS, Hunter K, et al. Assessment of skeletal muscle viability by PET. J Nucl Med. 1995; 36:1408–14. [PubMed: 7629586]

58. Abernathy VJ, Pou NA, Wilson TL, et al. Noninvasive measures of radiolabeled dextran transport in in situ rabbit lung. J Nucl Med. 1995; 36:1436–41. [PubMed: 7543146]

59. Lee RC, Myerov A, Maloney CP. Promising therapy for cell membrane damage. In: Lee RC, Capelli-Schellpfeffer M, Kelly KM, editorsAnn NY Acad Sci. Vol. 720. 1994. 239–45. Electrical injury: a multidisciplinary approach to therapy, prevention, and rehabilitation

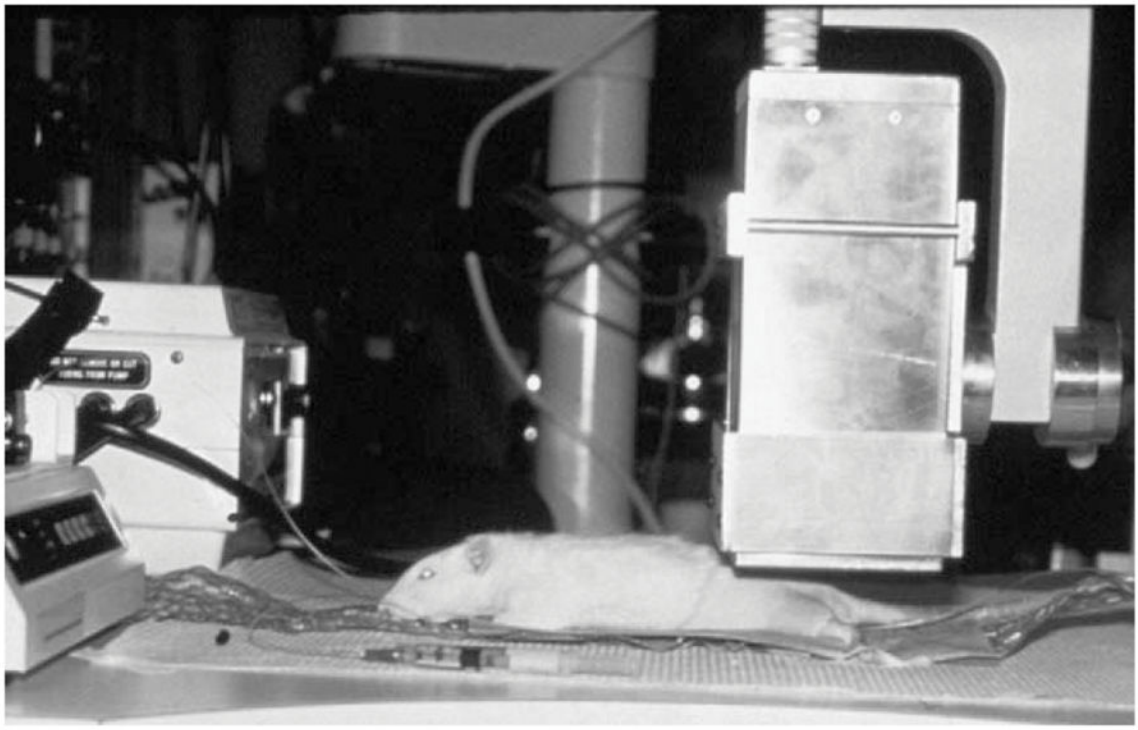

Fig. 1.

Photograph of the experimental setup, showing the anesthetized animal and the small gamma camera. The anesthetic infusion pump is seen at left and a syringe coupled to the jugular catheter is in the foreground; a pumped-water heating pad maintains the animal's body temperature.

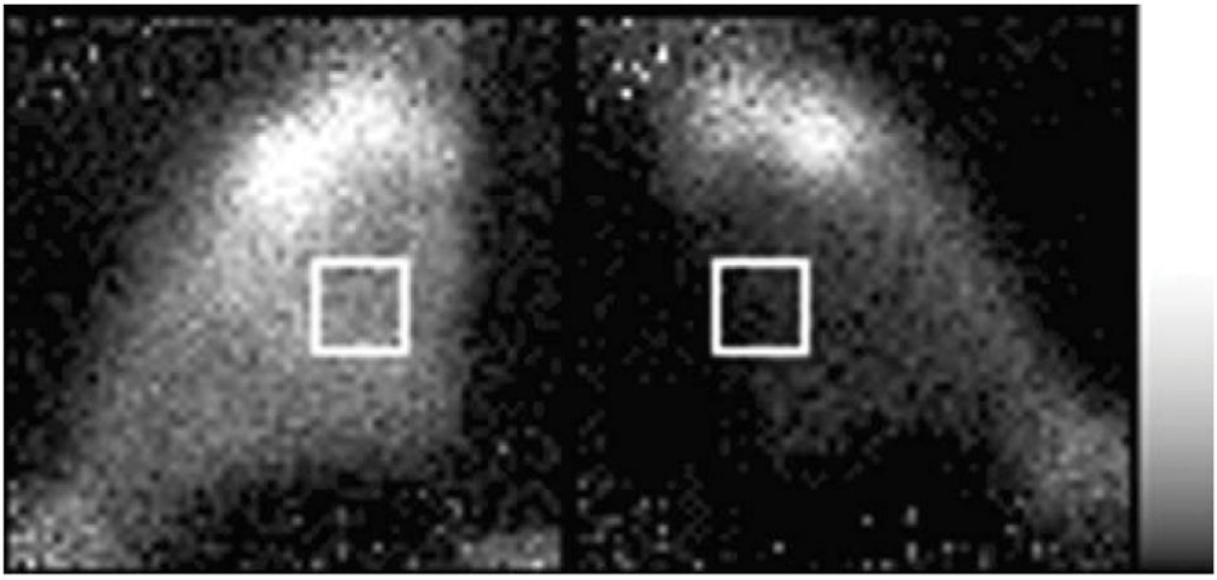

Fig. 2.

Typical posterior-view image of ^{99m}Tc PYP in the hind limbs. The left limb was shocked with 1.85 A pulses and ^{99m}Tc PYP was injected at 30 min post-shock. The left limb was imaged for 12 min at 105 min post-shock; the right limb was imaged for 12 min at 120 min post-shock. The muscle of the shocked limb (left) shows substantially more uptake than does the muscle of the unshocked limb (right). The white boxes illustrate the typical placement of ROIs over the muscle.

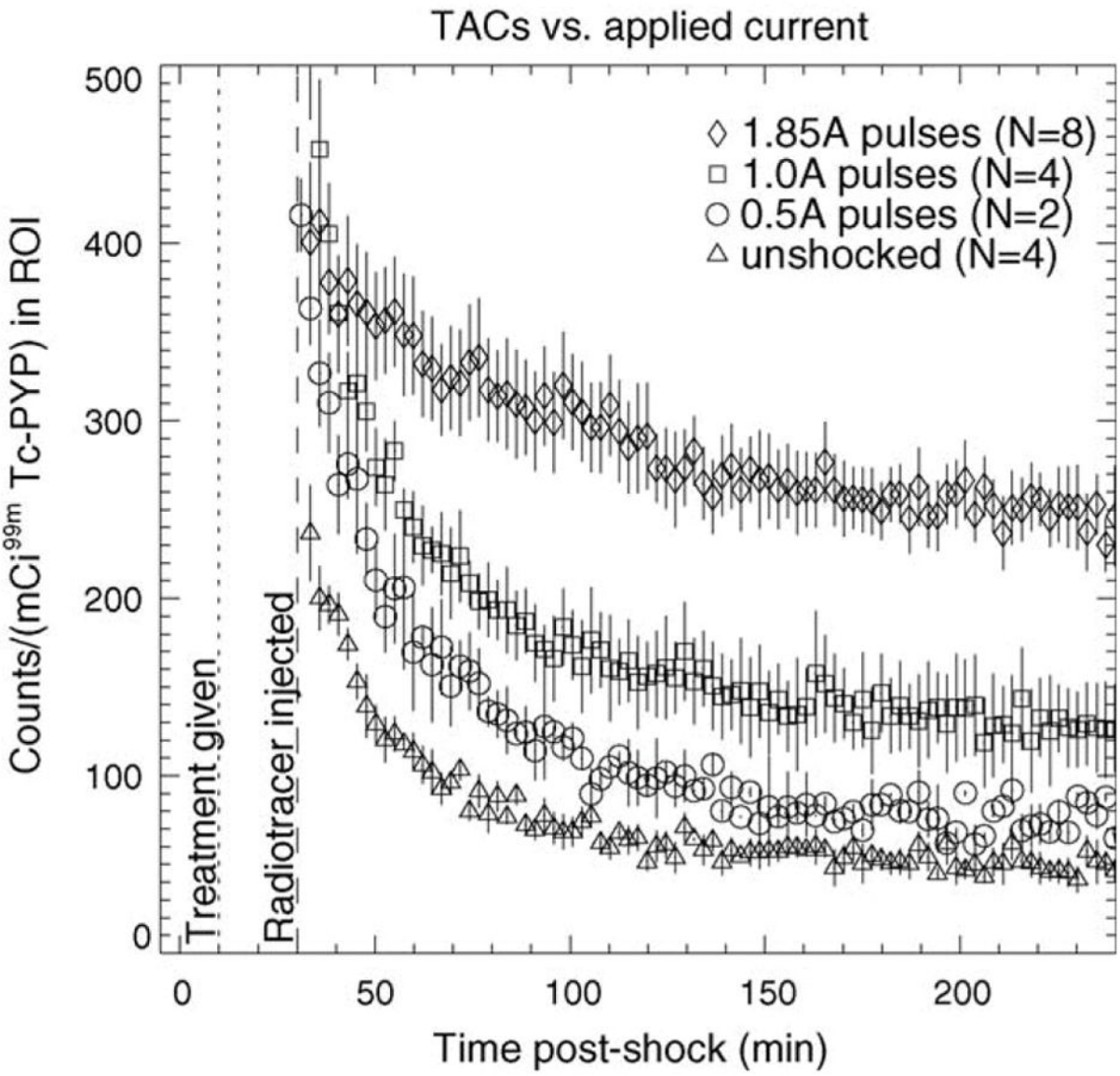

Fig. 3.

TACs for ^{99m}Tc PYP in saline-treated electroporated muscle vs. applied current. Saline was injected 10 min post-shock (dotted line) and radiotracer was injected 30 min post-shock (dashed line). Error bars represent S.E.M.

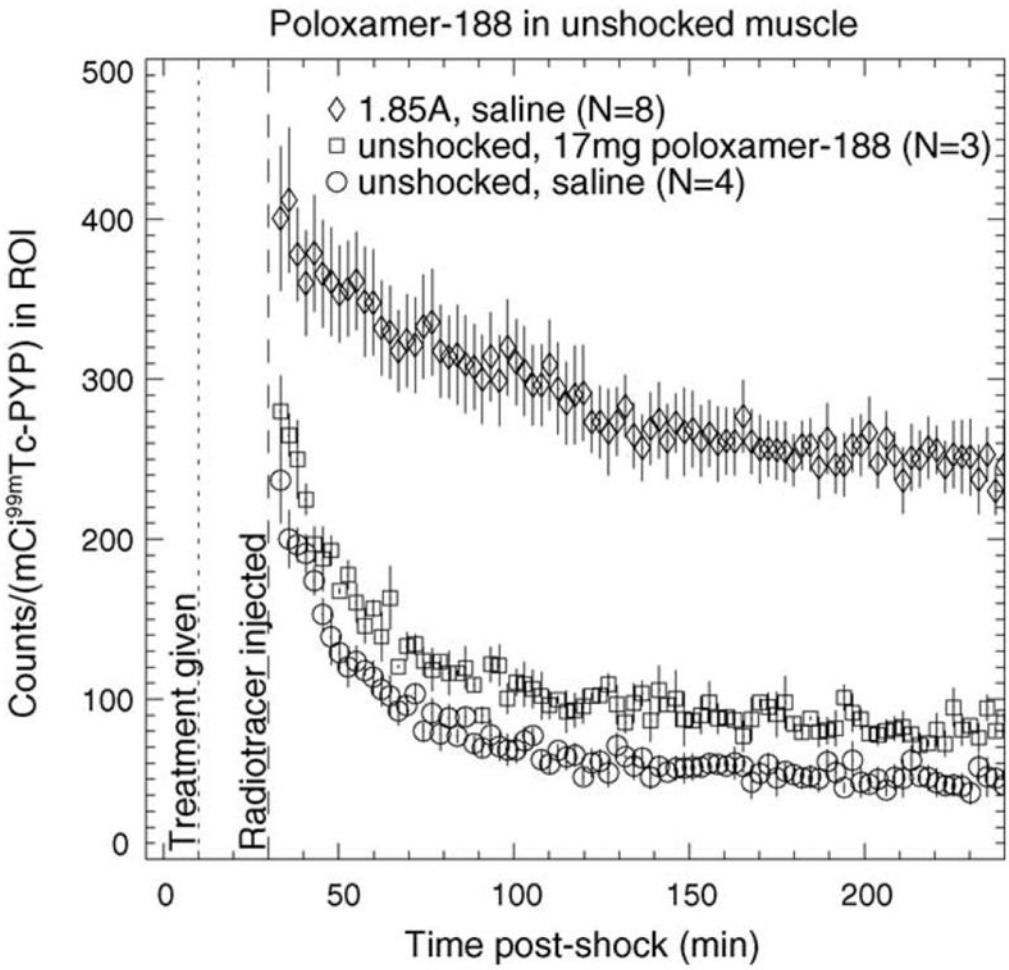

Fig. 4.

TAC of ^{99m}Tc PYP in unshocked muscle treated with 17 mg poloxamer-188. The TACs for unshocked saline-treated and 1.85 A-shocked saline-treated muscle are shown for comparison. Saline or polox-amer-188 was injected 10 min post-shock (dotted line) and radiotracer was injected 30 min post-shock (dashed line). Error bars represent S.E.M.

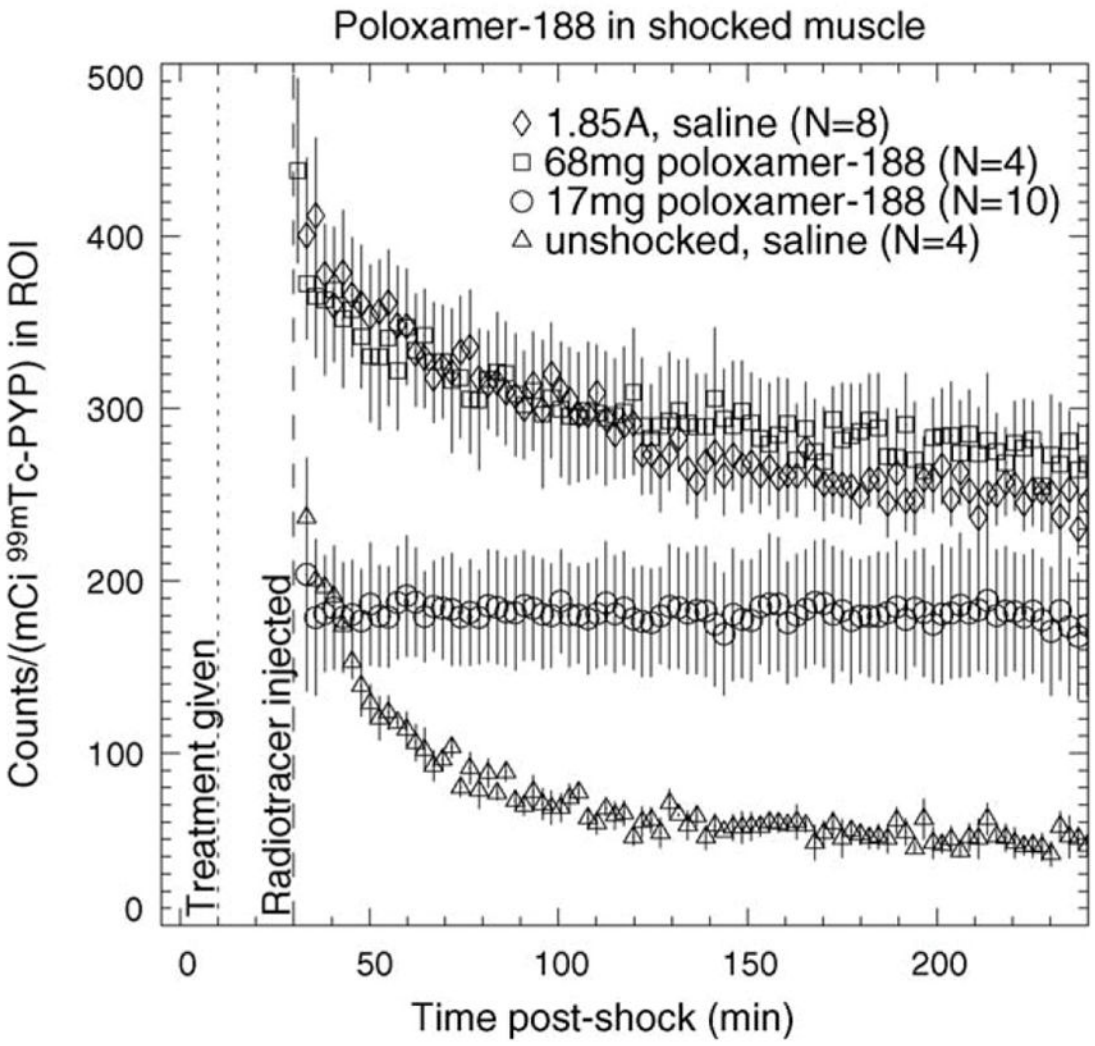

Fig. 5.

TACs of ^{99m}Tc PYP in poloxamer-188-treated electroporated muscle. TACs for unshocked saline-treated muscle and saline-treated muscle shocked at 1.85 A are shown for comparison. Therapeutic agent was injected 10 min post-shock (dotted line); radiotracer was injected 30 min post-shock (dashed line). Error bars represent S.E.M.

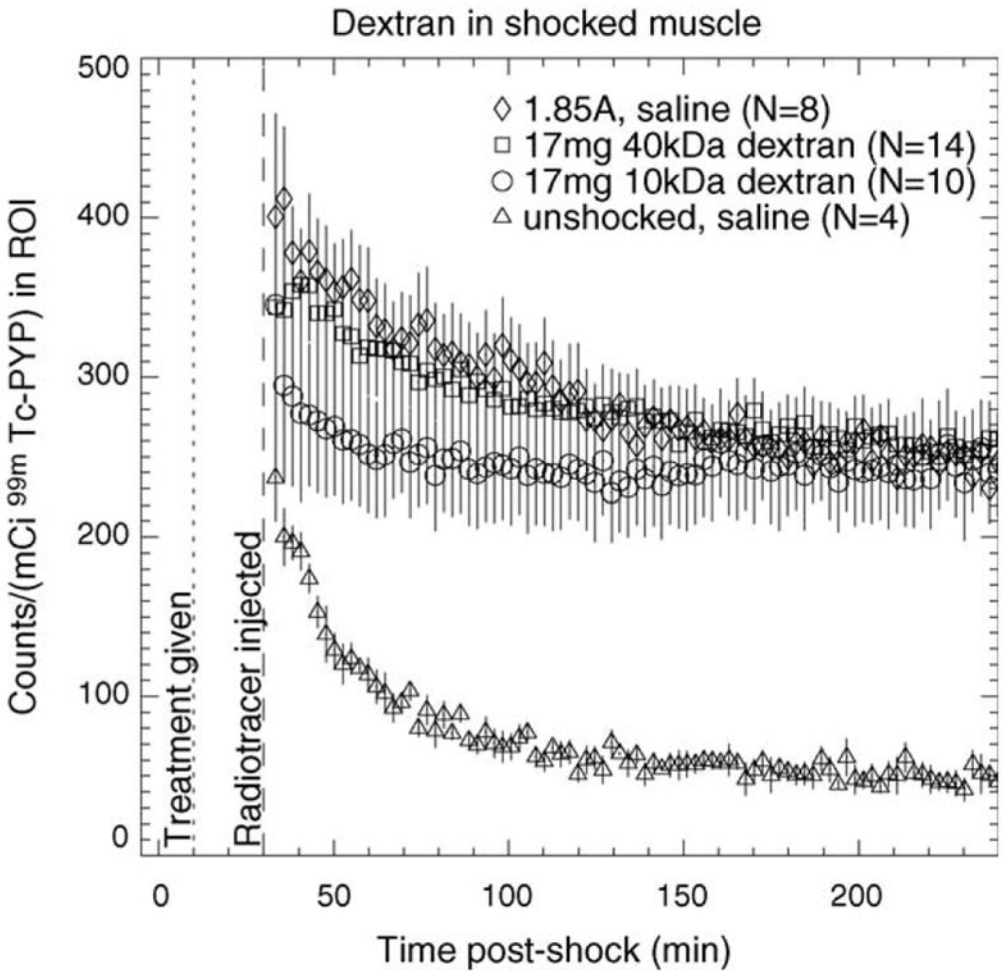

Fig. 6.

TACs of ^{99m}Tc PYP for 1.85 A-shocked electroporated muscle treated with 10 and 40 kDa dextran. TACs for unshocked saline-treated muscle and saline-treated muscle shocked at 1.85 A are shown for comparison. Therapeutic agent was injected 10 min post-shock (dotted line); radiotracer was injected 30 min post-shock (dashed line). Error bars represent S.E.M.

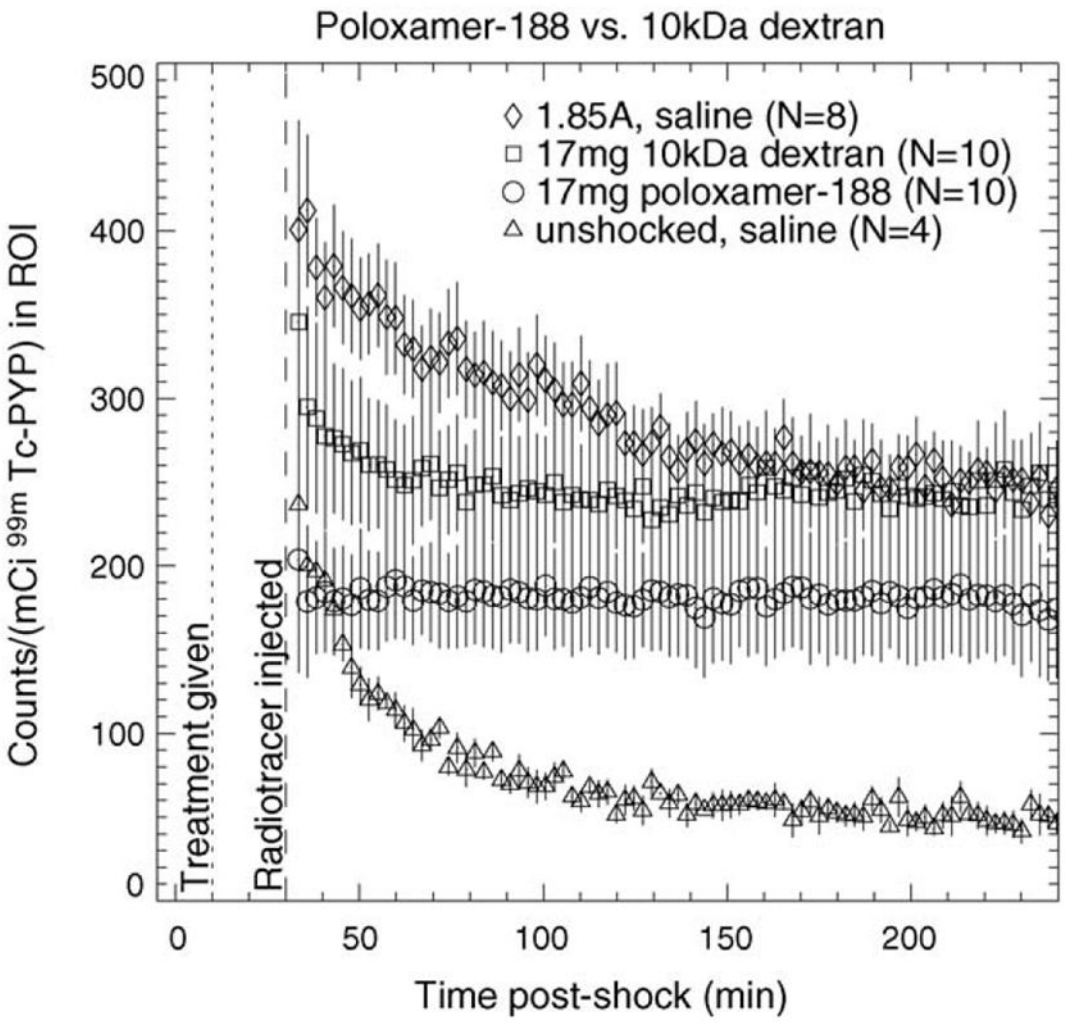

Fig. 7.

Comparison of TACs for treatment with 17 mg poloxamer-188 and 17 mg 10 kDa dextran. The TACs for 1.85 A-shocked and unshocked muscle treated with saline are shown for comparison. Therapeutic agent was injected 10 min post-shock (dotted line); radiotracer was injected 30 min post-shock (dashed line). Error bars represent S.E.M.

Table 1

Summary of experimental parameters

Common parameters				
Pulse sequence				
12 constant-current pulses				
4 ms duration each				
Field strength of ~150 V/cm in hind limb				
10 s interval between pulses				
Injection times				
Therapeutic agent: 10 min post-shock				
Radiotracer: 30 min post-shock				
Radiotracer				
^{99m}Tc pyrophosphate				
Nominal injected activity: 37 ± 7.4 MBq (1.0 ± 0.2 mCi)				
Image acquisition				
2 min duration for each image				
New image starting every 2.4 min				
~3.5 h (88–90 images)				
Experimental group name[a]	No. of rats	Shocked? (current)	Therapeutic agent	
			Type	Amount[b] (blood conc[c])
0 A saline	4	No	Saline	–
0 A 17 mg poloxamer-188	3	No	Poloxamer-188	17 mg (1 mg/ml)
0.5 A saline	2	Yes (0.5 A)	Saline	–
1.0 A saline	4	Yes (1.0 A)	Saline	–
1.85 A saline	8	Yes (1.85 A)	Saline	–
1.85 A 17 mg poloxamer-188	10	Yes (1.85 A)	Poloxamer-188	17 mg (1 mg/ml)
1.85 A 68 mg poloxamer-188	4	Yes (1.85 A)	Poloxamer-188	68 mg (4 mg/ml)
1.85 A 17 mg 10 kDa dextran	10	Yes (1.85 A)	10 kDa dextran	17 mg (1 mg/ml)
1.85 A 17 mg 40 kDa dextran	14	Yes (1.85 A)	40 kDa dextran	17 mg (1 mg/ml)

[a] Designated by applied current and therapeutic agent.

[b] Dissolved in 0.4 ml of saline.

[c] Assuming an average blood volume of 17 ml.

Table 2

ROI-derived fitted time-activity curve parameters

Experimental group[a]	Fitting parameter[b]		
	A^c	B^d	C^c
0 A saline	538.5	0.0359	53.0
1.85 A saline	251.1	0.0146	239.3
1.85 A 17 mg poloxamer-188	24.0	0.0021	162.5
1.85 A 68 mg poloxamer-188	195.2	0.0193	274.1
1.85 A 17 mg 10-kDa dextran	966.2	0.0781	244.9
1.85 A 17 mg 40 kDa dextran	174.6	0.0151	250.2
0 A 17 mg poloxamer-188	696.7	0.0409	87.0

[a] Designated by applied current and therapeutic agent.

[b] Exponential decay + constant background model: $f(t) = A \exp(-Bt) + C$.

[c] Magnitude; in units of counts in ROI per 2-min image.

[d] Decay constant; in units of min^{-1}.

Table 3

Statistical significance of fitted TAC parameters

For experimental group	Compared to	*p*-Value[a,b]		
		A	***B***	***C***
1.85 A saline	1.85 A 17 mg poloxamer-188	0.035	0.856	0.023
	1.85 A 68 mg poloxamer-188	0.271	0.569	0.912
	1.85 A 17 mg 10 kDa dextran	0.217	0.360	0.845
	1.85 A 17 mg 40 kDa dextran	0.775	0.335	0.905
	0 A 17 mg poloxamer-188	0.125	0.244	**0.003**
	0 A saline	0.132	0.177	**0.0003**
0 A saline	1.85 A 17 mg poloxamer-188	**0.0003**	0.544	**0.0004**
	1.85 A 68 mg poloxamer-188	**0.006**	0.036	**0.0001**
	1.85 A 17 mg 10 kDa dextran	0.419	0.774	**0.006**
	1.85 A 17 mg 40 kDa dextran	0.038	0.016	**0.0002**
	0 A 17 mg poloxamer-188	0.798	0.979	0.020
1.85 A 17 mg poloxamer-188	1.85 A 68 mg poloxamer-188	0.027	0.642	**0.007**
	1.85 A 17 mg 10 kDa dextran	0.241	0.521	0.136
	1.85 A 17 mg 40 kDa dextran	0.019	0.394	0.029
	0 A 17 mg poloxamer-188	**0.0001**	0.610	**0.007**
1.85 A 68 mg poloxamer-188	1.85 A 17 mg 10 kDa dextran	0.325	0.388	0.810
	1.85 A 17 mg 40 kDa dextran	0.274	0.847	0.833
	0 A 17 mg poloxamer-188	**0.002**	0.065	**0.0009**
1.85 A 17 mg 10 kDa dextran	1.85 A 17 mg 40 kDa dextran	0.111	0.129	0.902
	0-A 17-mg poloxamer-188	0.496	0.803	0.033
1.85 A 17 mg 40 kDa dextran	0 A 17 mg poloxamer-188	0.036	0.033	**0.003**

[a] *p*-Value for Student's *t*-statistic computed between the corresponding pair of fitted parameter values for the two datasets indicated.

[b] Bold values indicate the corresponding pair of fitted parameters is significantly different at the $p < 0.01$ level.